Cu Kα resonant x-ray emission spectroscopy of high-T_c-related cuprates

A. Kotani*
Photon Factory, Institute of Materials Structure Science, High Energy Accelerator Research Organization, 1-1 Oho, Tsukuba, Ibaraki 305-0801, Japan

K. Okada†
The Graduate School of Natural Science and Technology, Okayama University, 3-1-1 Tsushima-naka, Okayama 700-8530, Japan

György Vankó
European Synchrotron Radiation Facility, Boîte Postale 220, F-38043 Grenoble Cedex 9, France

G. Dhalenne and A. Revcolevschi
Laboratoire de Physico-Chimie de l'Etat Solide, UMR 8182, Université Paris-Sud, 91405 Orsay, France

P. Giura and Abhay Shukla
UMR7590, IMPMC, Université Pierre et Marie Curie-Paris 6,140 Rue de Lourmel, Paris F-75015, France
(Received 17 February 2008; revised manuscript received 21 April 2008; published 20 May 2008)

The pre-edge structure of Cu 1*s* excitations of high T_c cuprates reflects the lowest-lying unoccupied electronic states in these materials, and thus it is directly relevant to the interesting low-energy excitations and their nonlocal characters. We have performed theoretical calculations of the Cu Kα resonant x-ray emission spectroscopy (RXES) in the pre-edge region of La_2CuO_4 with a Cu_5O_{16} cluster model in order to analyze recent experimental data. The Cu 1*s* to on-site Cu 3*d* excitation by the electric quadrupole transition and the Cu 1*s* to off-site Cu 3*d* excitation by the electric dipole transition are taken into account, confirming that the off-site transition is indeed visible but that it is split due to the effect of both the local and the nonlocal components of screening. The calculated results of RXES spectra, as well as of x-ray absorption spectra by partial fluorescence yield method, are in reasonable agreement with the experimental data. The influence of the low-energy tail of Cu 4*p* states and the effects of doping electrons and holes are also calculated and discussed. Calculations are made for Cu Kα RXES of one-dimensional corner and edge sharing cuprates and compared to new experimental results for Sr_2CuO_3 and $GeCuO_3$.

DOI: 10.1103/PhysRevB.77.205116 PACS number(s): 71.15.Qe, 78.70.Ck, 74.72.Dn, 78.70.Dm

I. INTRODUCTION

Resonant x-ray emission spectroscopy (RXES) is a powerful tool in the study of electronic states of various materials.[1,2] Recent experiments on the RXES of correlated charge transfer insulators have made it possible to accurately measure structures associated with the pre-edge region of the absorption spectrum and with high resolution.

Shukla *et al.*[3] recently measured the Cu 1*s* x-ray absorption spectra (XAS) due to the partial fluorescence yield method (XAS-PFY) and the Cu Kα RXES spectra of La_2CuO_4, where a Cu 1*s* electron is excited to a pre-edge region and then a Cu 2*p* electron radiatively decays to the 1*s* state. They also made a theoretical analysis of the experimental data by combining calculations with *ab initio* energy band model and a CuO_4 cluster model. They showed that the Cu Kα RXES is an ultrafine probe of the Cu 1*s* pre-edge structures, which consist of the electric quadrupole (EQ) transition of a Cu 1*s* electron to the on-site Cu 3*d* states and the electric dipole (ED) transition to the "off-site Cu 3*d* states," i.e., Cu 3*d* states on the different atomic sites from the core excited site. The ED transition from Cu 1*s* to off-site 3*d* states is weakly allowed in the pre-edge region due to the hybridization between Cu 4*p* and the neighboring O 2*p* states and that between the O 2*p* and the neighboring Cu 3*d* states, whereas the Cu 1*s* to 4*p* ED transition is strong and forms the main absorption band. These pre-edge structures are directly relevant to the low-energy excitations of the highly correlated system, having bearings on important properties of the material, such as the nature of the charge transfer bands or the insulator-metal transition on doping. It is thus important to reach a more accurate theoretical description of the measured quantities and this is the main motivation of the present paper.

Before Shukla *et al.*,[3] similar Cu 1*s* XAS-PFY and Cu Kα RXES measurements were made for CuO and $Nd_{2-x}Ce_xCuO_4$ by Hayashi *et al.*[4,5] and for CuO by Döring *et al.*[6] For CuO, Hayashi *et al.*[4,5] and Döring *et al.*[6] observed a similar Cu Kα RXES structure to the off-site Cu 3*d* excitation by Shukla *et al.*,[3] but they did not discuss the microscopic mechanism of the spectral structure. In order to establish the off-site Cu 3*d* excitation mechanism, it would be necessary to perform a more detailed study from both experimental and theoretical sides.

In the present paper, we develop the theoretical calculations by using a two-dimensional (2D) Cu_5O_{16} cluster model,[7,8] instead of the previous CuO_4 cluster,[3] so that we can treat the on-site Cu 3*d* and off-site Cu 3*d* states on equal footing by fully taking the correlation effect into account.[9] The Cu 1*s* XAS-PFY and Cu Kα RXES spectra are calcu-

lated by exact diagonalization method.[7,8] With the Cu_5O_{16} cluster model, it is shown that after the off-site Cu 3*d* excitation, a core hole charge left behind is screened by the nonlocal charge transfer (the charge transfer between the neighboring CuO_4 plaquettes), which cannot be treated with CuO_4 model and only approximately treated in the previous paper.[3]

As another important object of this paper, the theory is extended from La_2CuO_4 [square planer (2D) Cu_5O_{16} cluster] to other cuprate systems: one-dimensional (1D) Cu_5O_{16} cluster and electron-doped and hole-doped 2D Cu_5O_{16} clusters. New experimental data for Sr_2CuO_3 and $GeCuO_3$ are shown and compared to the theoretical calculation. We also study the effect of the low-energy tail of the Cu 4*p* band (denoted by the background) on the Cu 1*s* XAS-PFY and Cu Kα RXES spectra.

The organization of the present paper is as follows: In Sec. II, we show the experimental results of XAS-PFY and RXES for La_2CuO_4 and explain the single electron picture of the EQ and ED transitions based on the *ab initio* band calculation. In Sec. III, the results of the Cu_5O_{16} cluster model calculations for La_2CuO_4 is given, and in Sec. IV, it is shown that the off-site 3*d* excitation is split into two components due to the nonlocal and local screening effects and this situation is compared in 1D and 2D cuprate systems. We study in Sec. V the effect of the low-energy tail of Cu 4*p* density of states and, in Sec. VI, the effect of electron and hole doping on the RXES spectrum with the 2D Cu_5O_{16} cluster model. New experimental data are shown in Sec. VII for the Cu Kα RXES of Sr_2CuO_3 and $GeCuO_3$, and compared to theoretical calculations. Finally, Sec. VIII is devoted to discussions and concluding remarks.

II. EXPERIMENTAL RESULTS AND SINGLE ELECTRON PICTURE FOR ELECTRIC QUADRUPOLE AND ELECTRIC DIPOLE TRANSITIONS

Experimental setups and procedures of the previous measurements of Cu 1*s* XAS-PFY and Cu Kα RXES for La_2CuO_4 were described in Ref. 3. The new experiments on Sr_2CuO_3 and $GeCuO_3$ (shown in Sec. VII) were performed at beam line ID16 at the European Synchrotron Radiation Facility. The experimental setup was that of a Rowland circle spectrometer with a horizontal scattering plane by using a spherically focusing bent Si(444) analyzer. The absorption spectra were obtained by measuring the total fluorescence yield while the RXES spectra were obtained in the usual way by using the spectrometer for inelastic scans in the region of the Kα peak while varying the incident energy in the pre-edge region as for an absorption measurement. The samples used were single crystals grown with the traveling solvent floating zone method. The use of single crystals made it possible to align the polarization direction parallel to the direction of the structural units of interest, that is, the Cu-O chains and the ladders.

In Fig. 1, we show the experimental results[3] of XAS-PFY of La_2CuO_4 for σ (dashed curve) and π (solid curve) polarizations, where the σ and π polarizations, respectively, mean the cases where the incident polarization is parallel and perpendicular to the CuO_2 plane. In the measurements of XAS-PFY, the Cu Kα fluorescence intensity is observed by sweeping the incident x-ray energy. The resolutions of incident and emitted x-rays are both 1.0 eV. In Fig. 1, the σ and π polarized XAS-PFY spectra are normalized to their peak intensities. It is seen that the XAS-PFY spectrum with σ polarization has a low-energy tail and a small structure at about 8.978 eV originating from the EQ transition, but the π-polarized XAS-PFY spectrum does not exhibit the low-energy tail. Shukla *et al.*[3] measured the Cu Kα RXES spectra with the σ-polarized incident x-ray for the pre-edge region from 8.976 to 8.981 eV (shown with a rectangle in Fig. 1), and the results are shown in the right panel of Fig. 2. The base line of each RXES spectrum corresponds to the incident x-ray energy at which it was measured as seen on the XAS-PFY spectrum, as shown in the left panel of Fig. 2. The RXES spectra have been arbitrarily shifted such that the lowest-energy transfer peak originating from the resonant EQ excitation corresponds to the zero of the energy scale and

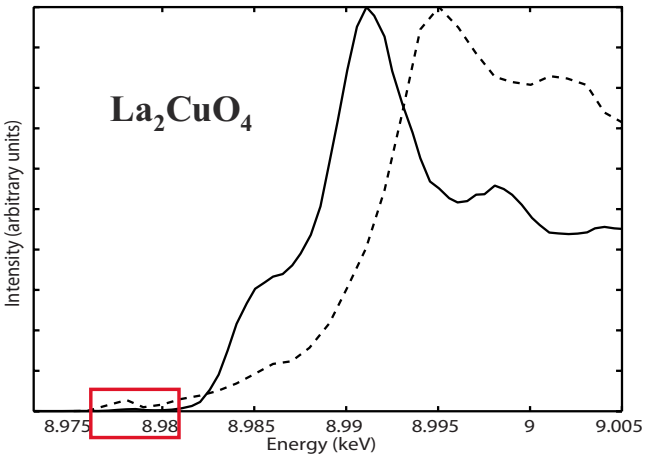

FIG. 1. (Color online) Experimental results of Cu 1*s* XAS-PFY. The dashed and solid curves correspond, respectively, to the σ and π polarizations. A small rectangle in the pre-edge region represents the energy range where the Cu Kα RXES is measured.

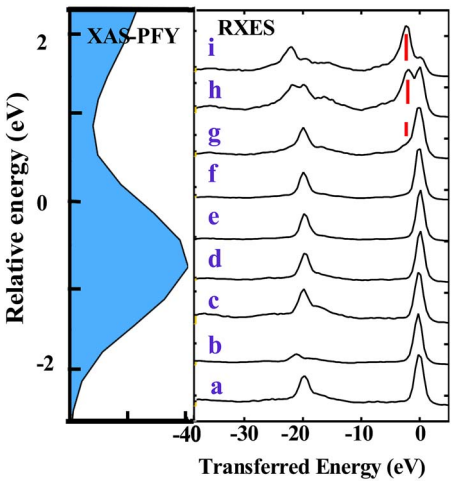

FIG. 2. (Color online) Cu Kα RXES spectra in the pre-edge region of La_2CuO_4 (right panel). The XAS-PFY spectrum for the σ polarization is also shown in the left panel.

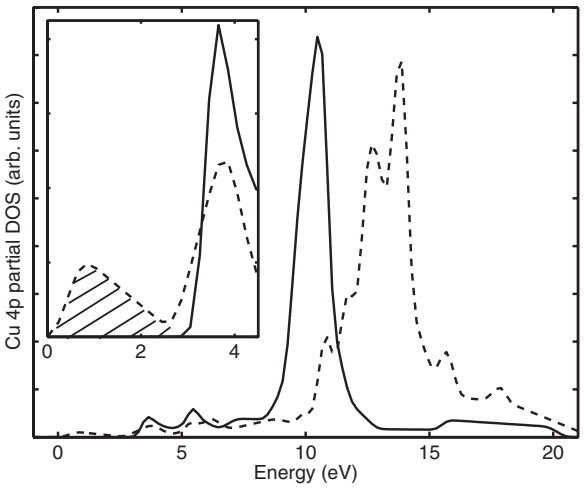

FIG. 3. Projected Cu $4p_\sigma$ (dashed curve) and $4p_\pi$ (solid curve) DOS calculated *ab initio*. The inset shows the low-energy region in detail. The hatched peak is the lowest-energy structure in the Cu $4p_\sigma$ DOS.

have been normalized to the most intense feature in each spectrum.

The RXES spectra show twin features separated by 20 eV due to spin-orbit splitting of the $2p$ core level, and we confine ourselves into the region from 0 to −10 eV (the $2p_{3/2}$ component). The Cu $2p_{3/2}$ state will be written simply as the Cu $2p$ state hereafter. It is to be noted that for three highest incident energies an additional feature indicated by a vertical bar occurs close to the 0 eV peak. This suggests the existence of a lowest-lying ED excitation at these incident energies, but the character of the ED excitation has not been known so far.

In order to see the mechanism of the lowest-lying ED excitation, Shukla *et al.*[3] investigated, by *ab initio* energy band calculations, the p-symmetric unoccupied state, which is allowed by the ED transition from the Cu $1s$ state. Figure 3 shows the calculated results of the projected Cu $4p_\pi$ (solid curve) and $4p_\sigma$ (dashed curve) density of states (DOS), and the inset shows the low-energy region in detail. It is seen that the hatched peak is the lowest-energy structure in the Cu $4p_\sigma$ DOS, which is located just above the Fermi energy (origin of the energy scale). The energy position of the hatched peak corresponds to the upper Hubbard band, but the on-site Cu $1s$-$3d$ transition is the ED forbidden transition, and the lowest ED transition is that from the Cu $1s$ state to the Cu $3d$ states on the different Cu sites (so that these Cu $3d$ states are denoted by "off-site Cu $3d$ states").

In Fig. 4, we schematically illustrate the off-site Cu $3d$ states with a Cu_5O_{16} cluster model. As shown on the right side of Fig. 4, the wave function of the off-site $3d$ state (with x symmetry) consists of the Cu $4p_x$ state on the central Cu site, O $2p_x$ states on the nearest neighboring O sites, and Cu $3d_{x^2-y^2}$ states on the next neighboring Cu sites (off-site Cu), which are coupled to each other by the Cu $4p$-O $2p$ and O $2p$-Cu $3d$ hybridization. The main weight of this wave function is on the off-site Cu $3d_{x^2-y^2}$ states, but this state is weakly allowed by the ED transition due to a small weight of the central Cu $4p_x$ state. The left hand side of Fig. 4 is the

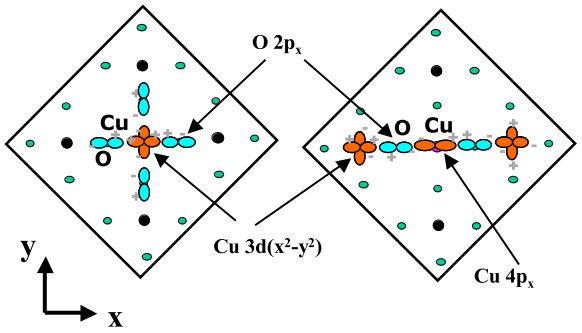

FIG. 4. (Color online) Schematic illustration of intermediate (and final) state of the Cu Kα RXES of cuprates with the Cu_5O_{16} cluster model. The ED-allowed off-site $3d$ state and the EQ-allowed on-site $3d$ state are shown, respectively, on the right and left hand sides.

on-site $3d$ state, which is allowed for the EQ excitation and mainly consists of the Cu $3d_{x^2-y^2}$ state on the central Cu site (the core hole site) but hybridized with the neighboring O $2p$ states.

In order to calculate the Cu Kα RXES spectrum, it is necessary to take into account the many-body effect beyond the energy band calculation. As a preliminary approach, Shukla *et al.*[3] calculated the RXES spectra with a CuO_4 cluster model combined with the σ-symmetric unoccupied states, and the results (not shown here) are consistent with the experimental data, confirming the Cu $1s$ to off-site $3d$ transition followed by the Cu $2p$-$1s$ x-ray emission as the mechanism of the new RXES peak. However, the CuO_4 cluster model is not sufficient in describing the many-body effects on the off-site $3d$ transition, and we will give below the results by Cu_5O_{16} cluster model calculations.

III. Cu_5O_{16} CLUSTER MODEL CALCULATIONS

We calculate the Cu Kα RXES spectra of La_2CuO_4 with the Cu_5O_{16} cluster model shown in Fig. 5(a). The Hamiltonian describing Cu $3d$ and O $2p$ states of the system is given, with the hole picture, by

$$H = \sum_{i,\sigma} \epsilon_d d^\dagger_{i,\sigma} d_{i,\sigma} + \sum_{j,\sigma} \epsilon_p p^\dagger_{j,\sigma} p_{j,\sigma} + \sum_{\langle i,j\rangle,\sigma} V_{pd,ij}(d^\dagger_{i,\sigma} p_{j,\sigma} + p^\dagger_{j,\sigma} d_{i,\sigma}) + \sum_{\langle j,j'\rangle,\sigma} V_{pp,jj'}(p^\dagger_{j,\sigma} p_{j',\sigma} + p^\dagger_{j',\sigma} p_{j,\sigma}) + U_{dd}\sum_i d^\dagger_{i,\uparrow} d_{i,\uparrow} d^\dagger_{i,\downarrow} d_{i,\downarrow} + U_{dc}\sum_\sigma d^\dagger_{0,\sigma} d_{0,\sigma} c^\dagger_0 c_0, \quad (1)$$

where $d^\dagger_{i,\sigma}(p^\dagger_{j,\sigma})$ creates a hole with spin σ on the ith Cu $3d_{x^2-y^2}$ orbit (the jth O $2p$ orbit). The first and second terms on the right hand side represent the one body energies, the third and fourth terms the hybridizations of the Cu $3d$ and O $2p$ orbits and of the neighboring O $2p$ orbits, respectively, and the fifth and sixth terms are Coulomb repulsion between Cu $3d$ holes and that between Cu $3d$ and core holes on the central Cu site. The operator $c^\dagger_0$ creates a core hole (a Cu $1s$ hole in the intermediate state and a Cu $2p$ hole in the

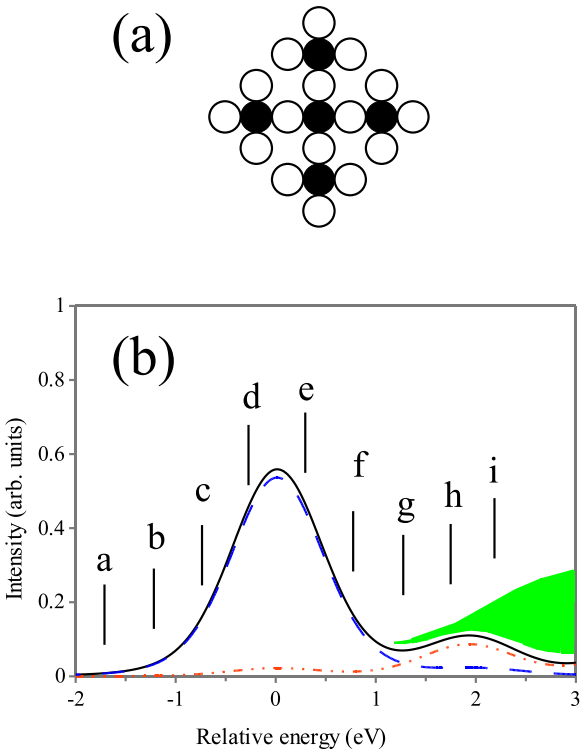

FIG. 5. (Color online) (a) The model of Cu_5O_{16} cluster and (b) the calculated result of the XAS-PFY spectra due to the EQ (dashed line), ED (chain line) transitions, and their sum (solid line). A possible low-energy tail of Cu $4p$ contribution is shown with the shaded part but disregarded in this calculation.

final state), and we assume that the core hole potential U_{dc} is the same for the Cu $1s$ and $2p$ core holes. The core hole creation energies [not written in Eq. (1)] are $|\epsilon_{1s}|$ (intermediate state) and $|\epsilon_{2p}|$ (final state), where ϵ_{1s} and ϵ_{2p} are the core electron energy levels.

The parameter values used are as follows: $pd\sigma=-1.5$ V, $pp\sigma=0.5$ eV, $U_{dd}=8.0$ eV, $U_{dc}=7.0$ eV, and $\Delta(=\epsilon_p-\epsilon_d)=3.5$ eV. The number of holes (Cu $3d$ and O $2p$ holes) in our cluster is fixed to four down-spin and one up-spin holes, corresponding to the undoped system with antiferromagnetic order. The polarization of the incident photon is taken in the x direction, while the polarization of the emitted photon is not analyzed. In addition to the electronic states written in Eq. (1), we take into account a Cu $4p$ state on the central Cu site and the hybridization between the Cu $4p$ and neighboring O $2p$ states in order to treat the ED transition to the off-site $3d$ states. The role of the Cu $4p$ state is limited to the off-site $3d$ excitation, and its direct contribution to the Cu Kα RXES is removed from our calculated results. The relative intensity of the Cu $1s$ to $3d$ EQ transition and of that to the off-site Cu $3d$ ED transition is treated as an adjustable parameter to reproduce the experimental spectra. More details on these parameters will be described in Sec. VIIIA together with some discussions.

The Cu Kα RXES spectrum $F_0(\Omega,\omega)$ is calculated by the coherent second order optical formula as

$$F_0(\Omega,\omega)=\sum_j\left|\sum_i\frac{\langle j|T_2|i\rangle\langle i|T_1|g\rangle}{E_g+\Omega-E_i+i\Gamma_{1s}}\right|^2 \times\frac{\Gamma_{2p}/\pi}{(E_j+\omega-E_g-\Omega)^2+\Gamma_{2p}^2}, \quad (2)$$

where Ω and ω are, respectively, the incident and emitted x-ray energies, $|g\rangle$, $|i\rangle$, and $|j\rangle$ are the initial, intermediate, and final states of the material system, E_g, E_i, and E_j are their energies, Γ_{1s} and Γ_{2p} are the Cu $1s$ and $2p$ core hole lifetime broadenings in the intermediate and final states, respectively, and T_1 includes both ED and EQ transitions of the Cu $1s$ electron and T_2 represents the Cu $2p$-$1s$ ED transition. The values of $2\Gamma_{1s}$ and $2\Gamma_{2p}$ are taken as 1.5 and 0.6 eV, respectively. Since we assume that U_{dc} is the same for the Cu $1s$ and $2p$ core holes, the states $|i\rangle$ and $|j\rangle$ of the transition $\langle j|T_2|i\rangle$ are the same except for the core hole state, and $E_i-E_j=\epsilon_{2p}-\epsilon_{1s}$.

In Eq. (2), the effect of the spectral resolution is not taken into account. In our calculation, we consider the resolution of incident and emitted x-rays by introducing the Gaussian functions G_i and G_e and calculate the spectrum as

$$F(\Omega,\omega)=\int dx\int dy G_i(x-\Omega)F_0(x,y)G_e(y-\omega), \quad (3)$$

where we use the experimental resolution of 1.0 eV (full width at half maximum) for both incident and emitted x rays. The XAS-PFY spectrum is calculated from Eq. (3) as a function of Ω by fixing ω at the Cu Kα fluorescence energy $\epsilon_{2p}-\epsilon_{1s}$. The numerical calculations are made by the exact numerical diagonalization of the Hamiltonian (1).

The calculated Cu XAS-PFY spectra in the pre-edge region are depicted in Fig. 5(b), where the EQ and ED contributions are shown with the dashed and chain curves, respectively, and the sum of these contributions is shown with the solid curve. Compared to the experimental XAS-PFY spectrum (in Figs. 1 and 2), the intensity of the calculated spectrum is much weaker on the high-energy side of the pre-edge, but this is because the model of our calculation does not include the effect of the low-energy tail of the Cu $4p$ DOS. We denote the low-energy tail of the Cu $4p$ DOS as the background, and the experimental result suggests that the background contribution to the XAS-PFY would be schematically given by the shaded area in Fig. 5(b). We will discuss in more detail the background contribution to XAS-PFY and RXES in Sec. V.

The Cu Kα RXES spectra are calculated for the incident photon energies indicated with a–i in Fig. 2, which are also shown in Fig. 5(b). As shown in Fig. 6, the calculated RXES peaks due to the EQ and ED resonant excitations are in good agreement with the experimental ones in Fig. 2. It is to be emphasized that the XAS-PFY intensity by the ED transition to the off-site $3d$ states is too weak (and overlapped with the background) to be clearly seen in the experimental XAS-PFY spectrum, but the signature of this ED excitation to the off-site $3d$ states can be seen clearly as an additional peak in the Cu Kα RXES. The relative energy positions of the ED and EQ contributions in both XAS-PFY and RXES spectra

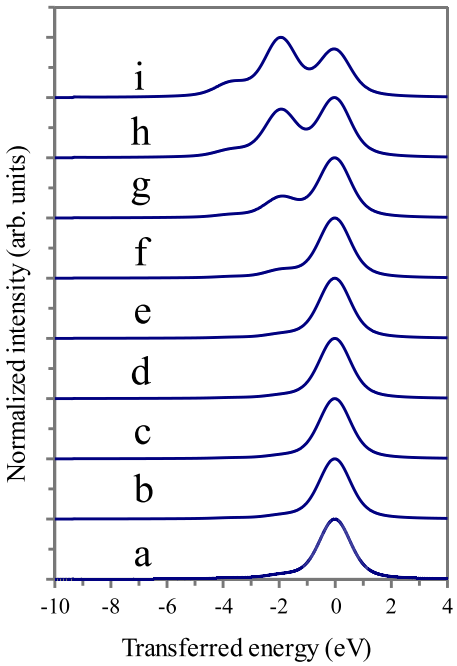

FIG. 6. (Color online) The calculated Cu Kα RXES spectra for the incident energy **a** to **i** indicated in Fig. 5(b).

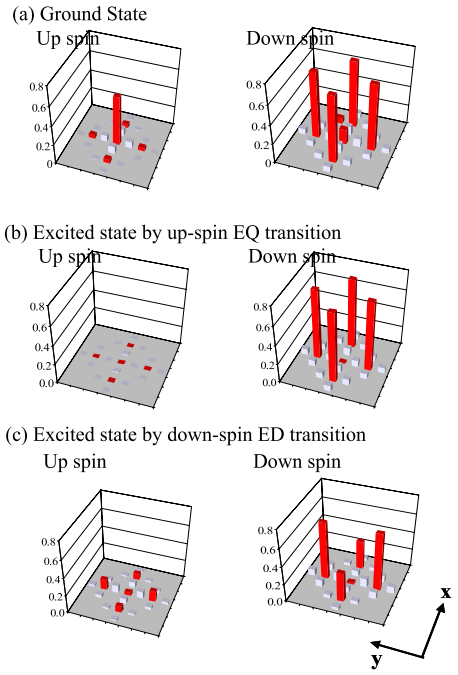

FIG. 7. (Color online) Spin-dependent hole distribution in the (a) ground, (b) EQ, and (c) ED excited states.

are naturally reproduced in the present calculation, although they were treated by introducing an adjustable parameter in the previous CuO_4 cluster model calculation.

In order to understand the electronic processes in the Cu Kα RXES and to get a proper insight into the screening effect accompanying the off-site 3*d* excitation, we calculate the spin-dependent hole distribution (for holes in the Cu 3*d* and O 2*p* states) over the five Cu sites and 16 O sites for the ground state and the EQ and ED excited states. In Fig. 7(a), the hole distribution in the ground state is shown for up-spin (left side) and down-spin (right side) states. It is seen that the up-spin hole is mainly located around the central Cu site and four down-spin holes are mainly located around the Cu sites in the neighboring CuO_4 plaquettes, corresponding to the antiferromagnetic order. In Fig. 7(b), we show the hole distribution in the excited state by the 1*s*-3*d* EQ transition of up-spin electron [excitation d and e in Fig. 5(b)]. By this transition, the valence holes with up spin are filled, so that almost no up-spin hole is left, while the distribution of down-spin holes is almost the same as that in the ground state. It is interesting to see the hole distribution in the excited state due to the ED transition of a down-spin electron from Cu 1*s* to the off-site 3*d* states [excitation h in Fig. 5(b)], as shown in Fig. 7(c). By the off-site ED transition due to the *x* polarized incident photon, the Cu 3*d* hole population in the neighboring CuO_4 plaquettes along the *x* direction is remarkably decreased. At the same time, the distribution of up-spin holes is strongly changed; the holes on the central Cu site is transferred mainly to the neighboring plaquettes to screen the core hole potential, which is denoted by the nonlocal screening effect. The up-spin holes transferred to the neighboring plaquette couple with the down-spin holes on the same plaquette to form the so-called Zhang–Rice singlet state [see Fig. 8(c)]. This nonlocal screening is very important to determine the relative energy of the EQ and ED excited states. It is to be noted that in the EQ excitation the core hole potential is well screened by the Cu 3*d* electron excited from the Cu 1*s* state, while in the ED excitation, it is screened by the charge transfer effect (nonlocal screening), and the energy difference between the EQ and ED excited states originates from the difference in the screening mechanisms of the core hole potential.

IV. NONLOCAL AND LOCAL SCREENINGS AND COMPARISON OF TWO-DIMENSIONAL AND ONE-DIMESIONAL SYSTEMS

In order to gain more insight into the spectral function $F(\Omega,\omega)$, we display the calculated result in the form of the 2D mapping, where we plot the spectral intensity as a contour map on the 2D plane spanned by the incident energy Ω and the energy transfer $\Omega-\omega$. The result is shown in Fig. 8(a), where we also extended the highest limit of the incident energy compared to that of Fig. 6. With this contour map, the Cu Kα RXES spectrum (as in Fig. 6) is obtained by the cross section along a constant incident energy line (as a function of the energy transfer), and the XAS-PFY [as in Fig. 5(b)] is obtained by the cross section along a diagonal line (a constant emitted x-ray energy line) passing through the EQ maximum point.

A new finding obtained from Fig. 8(a) is the existence of another RXES peak on the higher energy side of the off-site 3*d* contribution so far discussed. The new peak occurs at about 1.7 eV (transferred energy) above the previous off-site 3*d* peak with the incident energy tuned to about 1.7 eV above h of Fig. 5(b). Then, we calculate the spin-dependent hole distribution for this new peak, and the result is shown in

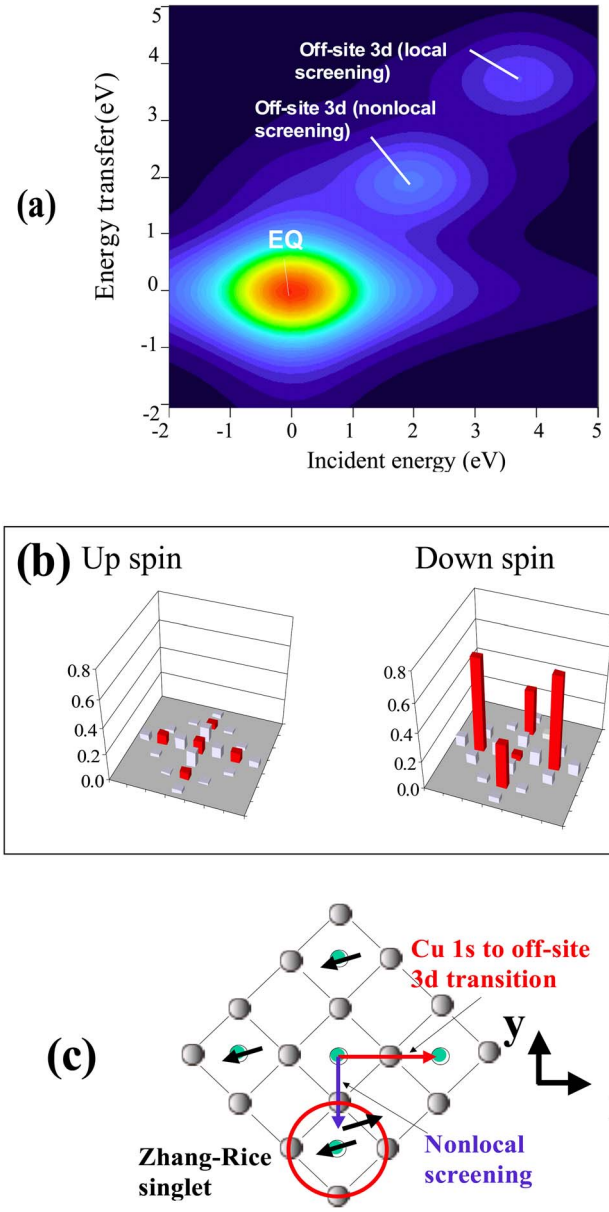

FIG. 8. (Color online) (a) Two-dimensional contour map of $F(\Omega,\omega)$ obtained with the Cu_5O_{16} cluster model calculation, (b) the spin-dependent hole distribution for the high-energy peak (due to the local screening effect) of the off-site 3*d* excitation, and (c) the schematic illustration of the Zhang–Rice singlet state formation by the nonlocal screening effect.

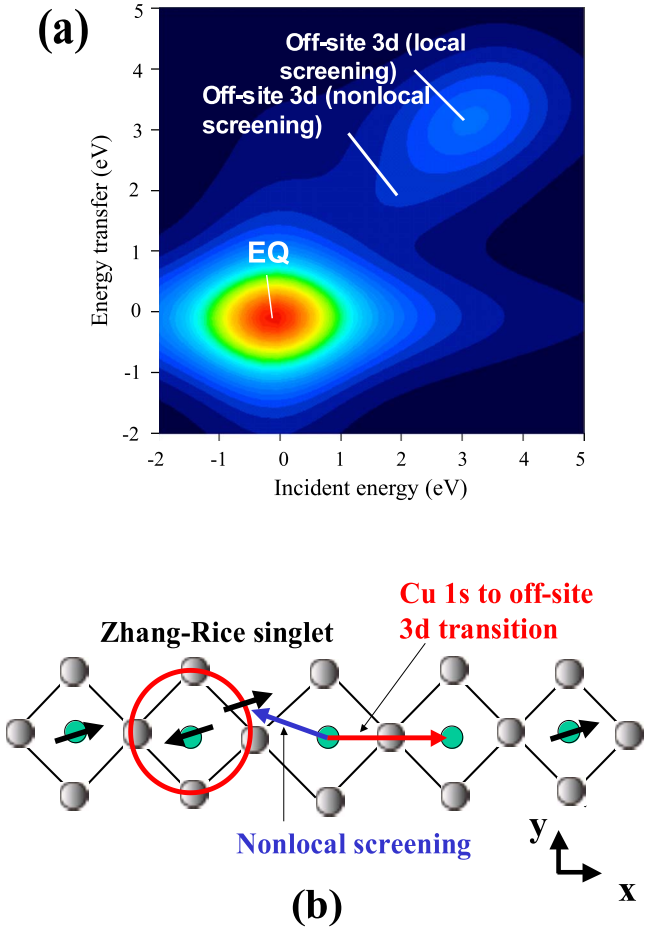

FIG. 9. (Color online) (a) Two-dimensional contour map of $F(\Omega,\omega)$ obtained with the 1D Cu_5O_{16} cluster model calculation and (b) the schematic illustration of the Zhang–Rice singlet state formation by the nonlocal screening effect.

Fig. 8(b). Comparing Fig. 8(b) to Fig. 7(c), we find that for Fig. 8(b) the up-spin hole distribution on the neighboring oxygen sites (with respect to the central Cu site) is larger than that on the Cu sites in the neighboring plaquette, which is opposite to the situation in Fig. 7(c). Therefore, we conclude that the local screening occurs for this new peak and that the off-site 3*d* excitation splits into two peaks depending on the nonlocal and local screening around the core hole. The excitation energy of the nonlocal screening state is lower than that of the local screening state because of the formation energy of the Zhang–Rice singlet state. The Zhang–Rice singlet formation process is illustrated in Fig. 8(c), where the arrow pointing right represents the excitation of the central Cu 1*s* electron to the off-site 3*d* state, and the arrow pointing downward stands for the nonlocal charge (hole) transfer from the central Cu site to the neighboring CuO_4 plaquette. The nonlocal screening results in the two holes bound as the Zhang–Rice singlet state on the neighboring plaquette. In the local screening state, on the other hand, the screening occurs mainly inside of the central plaquette, so that the Zhang–Rice singlet state cannot be formed. The nonlocal and local screening effects mentioned here are similar to those in the final state of Cu 2*p* x-ray photoemission spectroscopy (XPS) of cuprates, but the situation is somewhat different. This will be discussed in Sec. VIIB.

Stimulated by the novel many-body phenomena, such as the off-site 3*d* excitation, local and nonlocal screening effects, and Zhang–Rice singlet formation, which are characteristic of high T_c related cuprates, we extend our calculation of the Cu Kα RXES to the system of 1D cuprates, such as Sr_2CuO_3 with the Cu_5O_{16} cluster model shown in Fig. 9(b). The model parameter values are taken to be the same as those given in Sec. III for simplicity. The calculated spectra, $F(\Omega,\omega)$, is shown in Fig. 9(a) in the form of the 2D contour map. The result is similar to Fig. 8(a) for the 2D cuprates such as La_2CuO_4, but it is found that the intensity of the

nonlocal screening peak of the 1D system is weaker than that of the 2D system, while the intensity of the local screening peak is almost the same for the 1D and 2D systems. This result can be understood simply from a consideration on the dimensionality. If we compare Fig. 9(b) to Fig. 8(c), it is seen that in the 1D system, there is only one channel of the nonlocal screening to form the Zhang–Rice singlet state, while in the 2D system, we have three channels (upward, downward, and leftward hole-transfer channels). Therefore, the intensity of the nonlocal screening peak in the 1D system is about one-third of the 2D system. On the other hand, the local screening occurs mainly within the central CuO_4 plaquette, so that the intensity of the local screening peak is almost independent of the system dimension.

So far, the experimental measurement of the off-site $3d$ excitation has been made only for the nonlocal screening state of La_2CuO_4. It is very interesting to check the possibility of whether the nonlocal and local screening peaks can be observed for other 2D or 1D cuprate systems. In this respect, the influence of the low-lying Cu $4p$ states plays a key role, and we discuss this in Sec. V.

V. EFFECT OF LOW-ENERGY TAIL OF Cu $4p$ DENSITY OF STATES

Experimental result of the Cu $1s$ XAS-PFY of La_2CuO_4 suggests that the low-lying Cu $4p$ states (denoted by background) starts above the EQ excitation and its onset is very close to the off-site $3d$ excitation (see Figs. 1 and 2, and also the shaded spectral part in Fig. 5.) According to the energy band calculation (see Fig. 3), the onset of the off-site $3d$ state is just above the Fermi level (the lowest empty state), while the onset of the background is about 2 eV above the Fermi level. Therefore, there is no doubt that the off-site $3d$ excitation should be lower than the onset of the background, but the onset energy of the background would actually be lower than that of the band calculation.

In this section, we take into account the effect of the background with a simplified model. If we take only the one-electron Cu $1s$-$4p$ (background) and $2p$-$1s$ transitions and disregard all of the many-body effects, Eq. (2) is written as

$$F_0^{(BG)}(\Omega,\omega) = \int d\epsilon \rho(\epsilon) t_1^2 t_2^2 \times \frac{1}{(\Omega-\epsilon+\epsilon_{1s})^2+\Gamma_{1s}^2} \frac{\Gamma_{2p}/\pi}{(\Omega-\epsilon+\epsilon_{2p}-\omega)^2+\Gamma_{2p}^2}, \quad (4)$$

where $\rho(\epsilon)$ is DOS of the background and t_1 and t_2 are the amplitudes of Cu $1s$-$4p$ and $2p$-$1s$ dipole transitions. Actually, the many-body screening effect occurs after the Cu $1s$-$4p$ transition, but here we assume that $\rho(\epsilon)$ is the effective DOS including such a many-body effect. Then, we treat $t_1^2 t_2^2 \rho(\epsilon)$ as an appropriate model function, which starts from an appropriate onset energy and increases smoothly with increasing ϵ, so that the calculated XAS-PFY and RXES spectra can be consistent with the experimental ones.

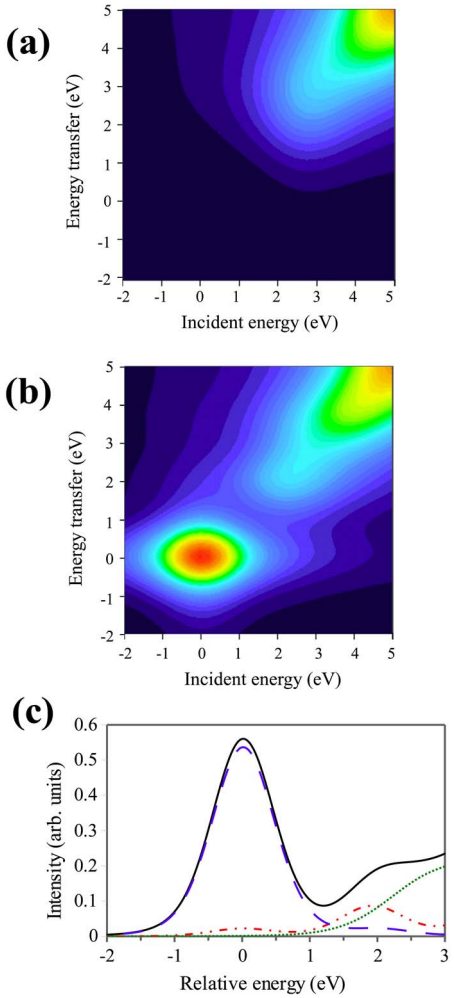

FIG. 10. (Color online) Two-dimensional contour map originating from (a) only the background and (b) all of EQ off-site $3d$ (ED) and background, calculated with the 2D Cu_5O_{16} cluster model. The Cu $1s$ XAS-PFY spectrum is shown in (c), where the EQ off-site ED and background contributions are shown with dashed, chain, and dotted curves, and the total sum is with the solid curve.

With this respect, the assumed function $t_1^2 t_2^2 \rho(\epsilon)$ is not unique, and, in this paper, we show a typical example of the effect of the background (actually we have tried various types of $t_1^2 t_2^2 \rho(\epsilon)$). In Fig. 10(a), we show the 2D contour map of $F(\Omega,\omega)$ originating only from the background contribution, which is obtained by putting Eq. (4) with an appropriate $t_1^2 t_2^2 \rho(\epsilon)$ into Eq. (3). Then, we superpose the 2D contour map of Fig. 8(a) with Fig. 10(a) and obtain the total 2D contour map of Fig. 10(b) including the background contribution.

It is confirmed that the off-site $3d$ excitation with the nonlocal screening can be well recognized even with the background contribution, but the local screening peak cannot be seen because of the overlap with the strong background contribution. Taking the cross section of Fig. 10(b) along the diagonal axis, we obtain the XAS-PFY spectrum, which is shown in Fig. 10(c) with the solid curve. The background contribution to XAS-PFY [the cross section of Fig. 10(a)] is also shown in Fig. 10(c) with the dotted curve. So long as the XAS-PFY spectrum is concerned, the separation of the off-

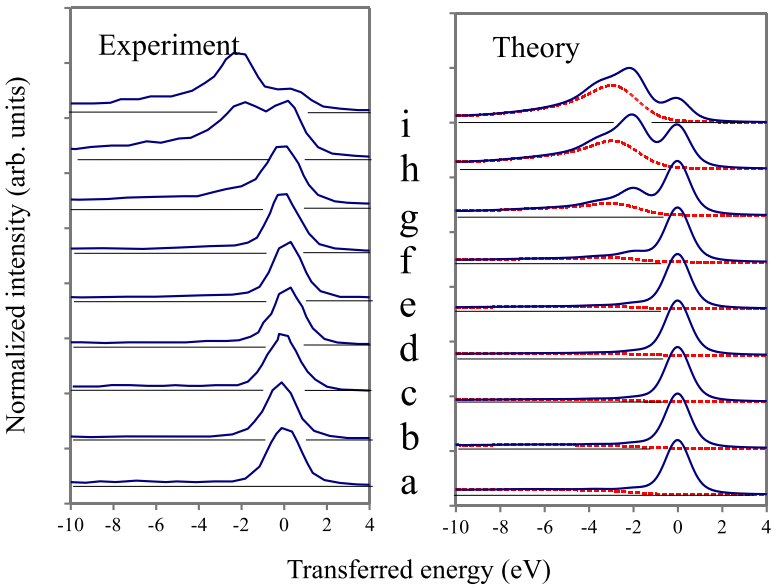

FIG. 11. (Color online) Theoretical (right) and experimental (left) results of the Cu Kα RXES spectra for La_2CuO_4. In the theoretical result, the background contribution is also shown with the dotted curves.

site 3*d* and background contributions is not very clear. On the other hand, the contribution of the off-site 3*d* excitation can be seen more clearly in the Cu Kα RXES spectra, i.e., by taking the cross section of Fig. 10(b) along the vertical axis (constant incident energy axis). Figure 11 (right) is the calculated Cu Kα RXES spectra (solid curves) for the incident energies a–i, as well as the background contribution (dotted curves), compared to the experimental results (left). It is seen that the background contribution is broader than the off-site 3*d* contribution and shifted to the lower transferred energy side by about 1 eV. It is to be remarked that the relative position of the EQ and off-site 3*d* excitation energies would be more or less common for various cuprates systems, but the onset of the background would strongly depend on the species of cuprates systems. In La_2CuO_4, the Cu 4*p* states hybridize with low-lying La 5*d* states to make lower the onset of the background. In any case, in order to detect the off-site 3*d* excitation with nonlocal and local screenings, it is important to select a cuprate system where the onset of the background is sufficiently high above the off-site 3*d* excitation.

VI. EFFECT OF ELECTRON AND HOLE DOPING WITH THE TWO-DIMESIONAL Cu_5O_{16} CLUSTER MODEL

The effect of the electron and hole dopings is calculated by changing the total hole number in the 2D Cu_5O_{16} cluster to 4 (20% electron doping) and to 6 (20% hole doping). The results of the 2D contour map of $F(\Omega,\omega)$ are shown in Fig. 12(a) for the 20% electron doping and in Fig. 12(b) for the 20% hole doping by including the background contribution, which is assumed to be the same as that of the undoped case [Fig. 10(a)]. By comparing the results of Figs. 12(a), 12(b), and 10(b), we find that the intensity of the off-site 3*d* (nonlocal screening) contribution decreases by doping electrons and increases by doping holes. The intensity of the EQ peak also changes by the carrier doping, especially by the electron doping. The effect of the carrier doping on the XAS-PFY spectra is calculated and shown in Fig. 13. Recently Hayashi *et al.*[10] measured the effect of the hole doping on the XAS-PFY spectra of La_2CuO_4 and observed the increase in the intensity in the region of higher energy than the EQ peak, which is in qualitative agreement with the present theoretical result. A more quantitative comparison is left for future investigations.

VII. EXPERIMENTAL RESULTS FOR ONE_DIMESIONAL CUPRATES

The condition that the off-site 3*d* excitation can be clearly measured in the Cu Kα RXES is (1) the intensity of the off-site 3*d* transition is not too small and (2) the off-site 3*d* transition is not overlapped with the strong background contribution. In the case of corner-sharing 1D cuprates, as we have shown in Sec. IV, the off-site 3*d* excitation would be observed if condition (2) is fulfilled. On the other hand, for edge-sharing 1D cuprates, the intensity of the off-site 3*d* transition would be too small because of the extremely weak interplaquette Cu 3*d*-O 2*p* hybridization strength so that the measurement of the off-site 3*d* transition would be impossible.

We have measured the Cu Kα RXES of a corner-sharing 1D cuprate Sr_2CuO_3 and an edge-sharing 1D cuprate $GeCuO_3$ and show the results in the form of 2D contour map in Figs. 14 and 15, respectively. The polarization of the incident photon is parallel to the 1D chain direction in both cases. Just looking at these contour map patterns, we see that the patterns of Sr_2CuO_3 and $GeCuO_3$ resemble, respectively, Figs. 10(b) and 10(a) [if we add the EQ contribution to Fig. 10(a)]. From the comparison of Figs. 14 and 9(a), we see that strong RXES spectra are observed in Sr_2CuO_3 near the position of the calculated off-site 3*d* contribution, but if we compare them more carefully, the observed intensity is too large to be attributed to the off-site 3*d* contribution. Therefore, we interpret that the observed RXES spectra of Sr_2CuO_3 is, except for the EQ contribution, mostly due to the background contribution, which is strong and starts from low onset energy. We consider that this strong low-lying back-

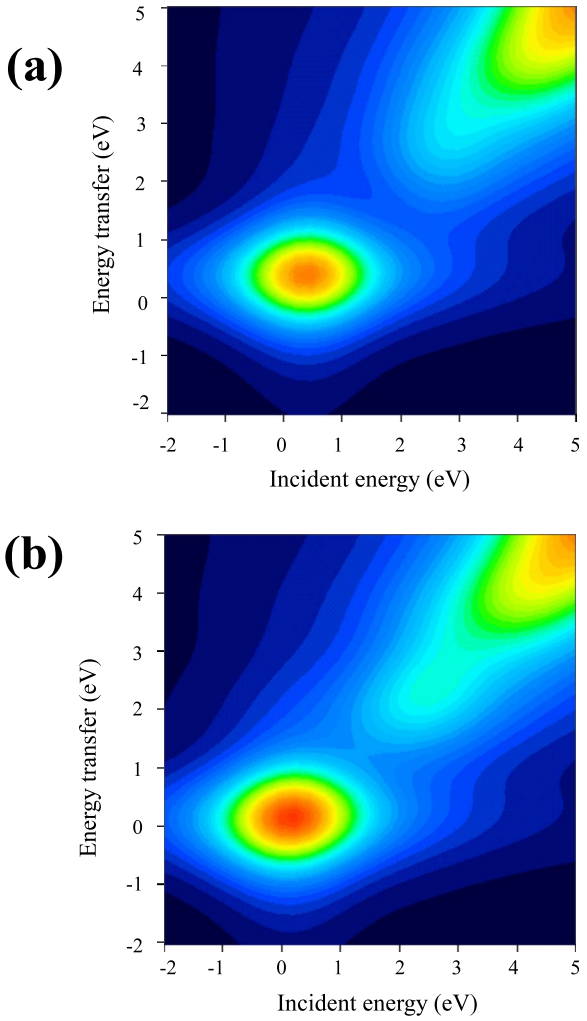

FIG. 12. (Color online) Two-dimensional contour map of $F(\Omega,\omega)$ calculated for (a) 20% electron doping and (b) 20% hole doping with the 2D Cu_5O_{16} cluster model including the background contribution.

ground of Sr_2CuO_3 originates mainly from the Sr 4*d* states with *p* symmetric DOS around the central Cu site. We believe that the off-site 3*d* contribution should exist near the bottom of the background contribution, but it cannot be separated from the background contribution.

For $GeCuO_3$, on the other hand, the onset of the background is sufficiently high so that if the off-site 3*d* contribution had some detectable intensity it would be measured separately from the background contribution. The experimental results of Fig. 15 confirms that the intensity of the off-site 3*d* transition in $GeCuO_3$ is vanishingly small because of the edge-sharing structure and it cannot be observed experimentally.

VIII. DISCUSSION AND CONCLUSION

A. Intensity of electric quadrupole and electric dipole transitions

In the present paper, the relative intensity of ED (a main 4*p* band and an off-site 3*d* excitation) and EQ transitions is

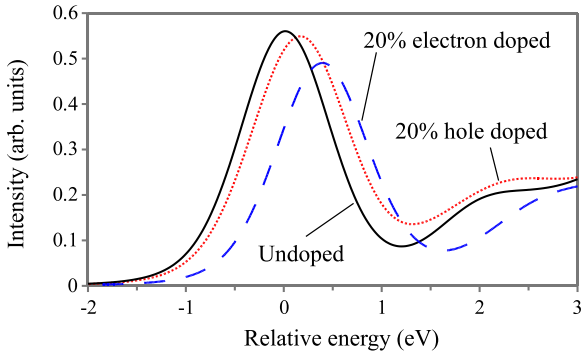

FIG. 13. (Color online) Calculated Cu 1*s* XAS-PFY spectra of undoped and 20% electron and hole doped systems with the 2D Cu_5O_{16} cluster model including the background contribution.

treated as an adjustable parameter to obtain the reasonable result compared to the experiments. The method of calculating the ED transition is mentioned here in some detail. As a simplified model of the Cu 4*p* main band (in the absence of the background), we assume, only on the central Cu site, a single Cu 4*p* level, which is located at 17 eV above the O 2*p* level, and take into account the Cu 4*p*-O 2*p* hybridization with $pp\sigma=2$ eV. Then, combining them with our 2D Cu_5O_{16} cluster model, we naturally obtain the off-site 3*d* transition with a finite intensity. This process is almost the same as introducing in the transition operator T_1 the Cu 1*s* to off-site 3*d* transition operator obtained by the second order perturbation Cu $1s \rightarrow$ Cu $4p \rightarrow$ O $2p \rightarrow$ Cu 3*d* with Cu 4*p* and O 2*p* states as virtual intermediate states. Quantitatively, with our parameter values, the relative transition intensity of the off-site 3*d* excitation and the main Cu 4*p* excitation is about 1/500, which is consistent with that estimated from the *ab initio* energy band calculation (see Fig. 3). When we introduce the background contribution, we assume an extra XAS band with an appropriate spectral shape and an appropriate intensity, as mentioned in Sec. V.

On the relative intensity of the ED and EQ transitions, we assume that the intensity ratio of the Cu 1*s* to 3*d* EQ transition and the Cu 1*s* to 4*p* (main line) transition is 1/100. This is consistent with a very rough estimation of atomic transition intensity. Then, it is found that the intensity ratio of the EQ transition and the ED off-site 3*d* transition is around 5.

B. Nonlocal and local screening effects

In Sec. IV, we have shown that the Cu Kα RXES peak of the off-site 3*d* excitation splits into two peaks due to the nonlocal and local screening effects. This situation is similar to that in the Cu 2*p* XPS, but, more exactly, the situation in Cu Kα RXES is somewhat different from that in Cu 2*p* XPS, especially for the "local" screening effect, as mentioned below. The splitting of a main peak of Cu 2*p* XPS is first explained by van Veenendaal and co-workers[11,12] with a linear chain Cu_3O_{10} cluster model; the lower binding energy peak (first peak) is due to the nonlocal screening, where a hole is transferred from the central Cu site to the neighboring CuO_4 plaquette to form the Zhang–Rice singlet state, and the higher binding energy peak (second peak) is due to the local

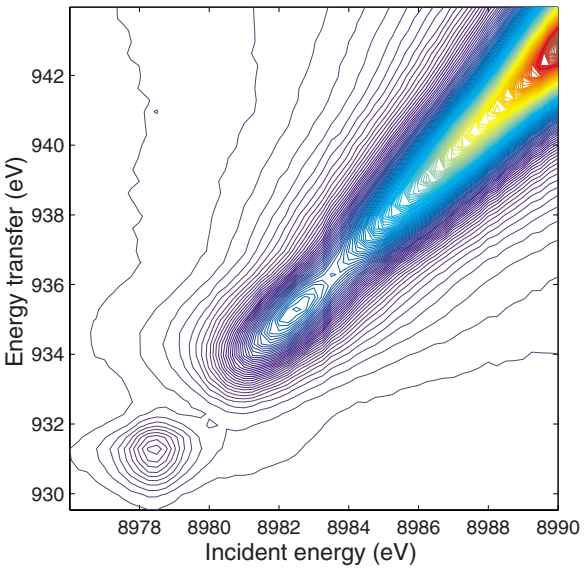

FIG. 14. (Color online) Experimental result of the two-dimensional contour map of the Cu Kα RXES of Sr_2CuO_3.

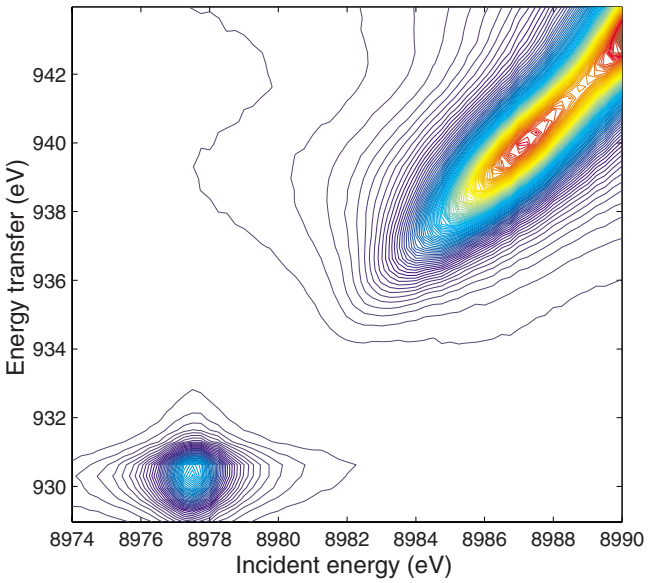

FIG. 15. (Color online) Experimental result of the two-dimensional contour map of the Cu Kα RXES of $GeCuo_3$.

screening, where the hole transfer is mainly from the central Cu site to the neighboring O sites (mainly to the boundary O sites perpendicular to the chain direction). After that, Okada and Kotani[13] studied the spatial distribution of the screening hole charge of Cu 2*p* XPS in the square planar Cu_5O_{16} cluster and pointed out that the hole distribution of the second peak is not localized within the central CuO_4 plaquette but even more delocalized than that of the first peak (nonlocal screening peak). Therefore, one cannot denote the second peak of Cu 2*p* XPS of 2D cuprates as "local" screening peak.

The situation is different from the splitting of the off-site 3*d* excitation peak in Cu Kα RXES. In contrast to the final state of Cu 2*p* XPS, we have one extra electron in the off-site 3*d* state (excited from the Cu 1*s* state) in Cu Kα RXES, but this extra electron prevents the screening hole from extending beyond the central CuO_4 plaquette, at least in the direction of the incident photon polarization. Therefore, the hole distribution of the second peak is considerably localized, as shown in Fig. 8(b) (up spin). This is why we have used the term "local screening" in the present paper. At the same time, we would like to remark that the term of local screening is sometimes used wrongly in describing the final state of Cu 2*p* XPS of 2D cuprates.

C. Off-site 3*d* excitation in transition metal compounds

We have shown that the lowest-lying ED transition of the Cu 1*s* electron of cuprates is the off-site 3*d* excitation. This situation should be commonly seen not only for cuprates but also for transition metal (TM) 1*s* excitations of various TM compounds, although the intensity of the off-site 3*d* transition is often very weak. A well known example is the Ti 1*s* excitation of TiO_2 (rutile). In the pre-edge region of the Ti 1*s* XAS of TiO_2, three peaks were measured by Grunes[14] more than 20 years ago (see also Refs. 15 and 16). The first theoretical interpretation of the three peaks was given by Uozumi *et al.*[16] According to their theory, two EQ transitions to the $3d(t_{2g})$ (lowest peak) and $3d(e_g)$ (middle peak) states and two ED transitions to the *off-site* $3d(t_{2g})$ (middle peak) and $3d(e_g)$ (highest peak) states should exist in the pre-edge region of the Ti 1*s* XAS, but the EQ transition to the $3d(e_g)$ state is overlapped with the ED transition to the off-site $3d(t_{2g})$ so that the three peaks are observed experimentally. Similar theoretical calculations were made more recently by Joly *et al.*[17] and by Shirley.[18] The evidence that the middle one of the three peaks consists of the EQ and off-site ED transitions overlapped each other is obtained by the resonant Auger electron experiment[19] and its theoretical analysis.[20,21]

It is to be mentioned that TiO_2 is the band-type insulator, where the insulating energy gap does not originate from the correlation gap. The off-site 3*d* transition in La_2CuO_4, which was measured by Shukla *et al.*[3] and analyzed in the present paper, is the first example that the ED transition is observed to the off-site 3*d* states just above the correlation gap. Other examples are similar off-site 3*d* transitions measured by Co Kα RXES of $EuCoO_3$ and $LaCoO_3$.[22,23] It is desirable that more precise experimental and theoretical investigations would be made for the off-site 3*d* transition in many other TM compounds.

D. Concluding remarks

We confirmed that the off-site ED transition detected by Shukla *et al.*[3] is visible in RXES measurements but also showed that higher resolution measurements should give evidence of a splitting of this transition due to the local and nonlocal contributions to the screening. These different screening mechanisms were discussed at length. Since the features discussed are generally weak, we made some rough estimates of relative intensities of the EQ on-site and the ED

off-site transitions. To be able to detect the off-site transitions, which should be present in most TM compounds, it is also important that other contributions in the DOS be absent in the same energy range. These considerations should provide basic guidelines for interpreting RXES spectra in TM compounds.

ACKNOWLEDGMENTS

We would like to thank M. Calandra, M. Taguchi, and S.-W. Cheong for their collaboration in the early stage of the present work. G.V. was supported by Hungarian Research Fund (OTKA) under Contract No. K 72597.

*Also at RIKEN Harima Institute, 1-1-1 Kouto, Sayo, Hyogo 679-5148, Japan; kotani@post.kek.jp

†Also at KFKI Research Institute for Particle and Nuclear Physics, P.O. Box 49, H-1525 Budapest, Hungary.

[1] A. Kotani and S. Shin, Rev. Mod. Phys. **73**, 203 (2001).

[2] A. Kotani, Eur. Phys. J. B **47**, 3 (2005).

[3] A. Shukla, M. Calandra, M. Taguchi, A. Kotani, G. Vankó, and S.-W. Cheong, Phys. Rev. Lett. **96**, 077006 (2006).

[4] H. Hayashi, Y. Udagawa, W. A. Caliebe, and C. C. Kao, Phys. Rev. B **66**, 033105 (2002).

[5] H. Hayashi, R. Takeda, M. Kawata, Y. Udagawa, Y. Watanabe, T. Takano, S. Nanao, N. Kawamura, T. Uefuji, and K. Yamada, J. Electron Spectrosc. Relat. Phenom. **136**, 199 (2004).

[6] G. Döring, C. Sternemann, A. Kaprolat, A. Mattila, K. Hämäläinen, and W. Schulke, Phys. Rev. B **70**, 085115 (2004).

[7] K. Okada and A. Kotani, J. Electron Spectrosc. Relat. Phenom. **86**, 119 (1997).

[8] K. Okada and A. Kotani, J. Phys. Soc. Jpn. **74**, 653 (2005).

[9] Preliminary results were partly reported in A. Kotani, K. Okada, M. Calandra, and A. Shukla, in *X-Ray Absorption Fine Structure — XAFS13*, edited by B. Hedman and P. Pianetta (AIP, Melville, NY, 2007), p. 99.

[10] H. Hayashi, T. Azumi, A. Sato, R. Takeda, M. Kawata, Y. Udagawa, N. Kawamura, K. Yamada, and K. Ikeuchi, Radiat. Phys. Chem. **75**, 1586 (2006).

[11] M. A. van Veenendaal and G. A. Sawatzky, Phys. Rev. Lett. **70**, 2459 (1993).

[12] M. A. van Veenendaal, H. Eskes, and G. A. Sawatzky, Phys. Rev. B **47**, 11462 (1993).

[13] K. Okada and A. Kotani, Phys. Rev. B **52**, 4794 (1995).

[14] L. A. Grunes, Phys. Rev. B **27**, 2111 (1983).

[15] B. Poumellec, R. Cortes, G. Tourillon, and J. Berthon, Phys. Status Solidi B **164**, 319 (1991).

[16] T. Uozumi, K. Okada, A. Kotani, O. Durmeyer, J. P. Kappler, E. Beaurepaire, and J. C. Parlebas, Europhys. Lett. **18**, 85 (1992).

[17] Y. Joly, D. Cabaret, H. Renevier, and C. R. Natoli, Phys. Rev. Lett. **82**, 2398 (1999).

[18] E. L. Shirley, J. Electron Spectrosc. Relat. Phenom. **136**, 77 (2004).

[19] J. Danger, P. Le Fèvre, H. Magnan, D. Chandesris, S. Bourgeois, J. Jupille, T. Eickhoff, and W. Drube, Phys. Rev. Lett. **88**, 243001 (2002).

[20] T. Uozumi, A. Kotani, and J. C. Parlebas, J. Electron Spectrosc. Relat. Phenom. **137-140**, 623 (2004).

[21] P. Le Fèvre, H. Magnan, D. Chandesris, J. Jupille, S. Bourgeois, W. Drube, H. Ogasawara, T. Uozumi, and A. Kotani, J. Electron Spectrosc. Relat. Phenom. **136**, 37 (2004).

[22] G. Vankó (unpublished).

[23] See also F. M. F. de Groot and A. Kotani, *Core Level Spectroscopy of Solids* (CRC, Boca Raton, FL/Taylor & Francis, London, 2008).